New Observations on Complex RTN in Scaled High-κ/Metal-gate MOSFETs – the Role of Defect Coupling under DC/AC Condition

Pengpeng Ren[1], Peng Hao[1], Changze Liu[1], Runsheng Wang[1]*, Xiaobo Jiang[1], Yingxin Qiu[1], Ru Huang[1]*, Shaofeng Guo[1], Mulong Luo[1], Jibin Zou[1], Meng Li[1], Jianping Wang[2], Jingang Wu[2], Jinhua Liu[2], Weihai Bu[2], Waisum Wong[2], Scott Yu[2], Hanming Wu[2], Shiuh-Wuu Lee[2], Yangyuan Wang[1]

[1] Institute of Microelectronics, Peking University, Beijing 100871, China (*emails: ruhuang@pku.edu.cn; r.wang@pku.edu.cn)
[2] Semiconductor Manufacturing International Corporation (SMIC), Shanghai 201203, China

Abstract

The coupling effect between multi-traps in complex RTN is experimentally studied in scaled high-κ/metal-gate MOSFETs for the first time. By using extended STR method, the narrow "test window" of complex RTN is successfully expanded to full V_G swing. Evident defect coupling can be observed in both RTN amplitude and time constants. Interesting nonmonotonic bias-dependence of defect coupling is found, which is due to two competitive mechanisms of Coulomb repulsion and channel percolation conduction. The decreased defect coupling is observed with increasing AC frequency. Based on the new observations on complex RTN, its impacts on the circuit stability are also evaluated, which show an underestimation of the transient performance if not considering defect coupling. The results are helpful for future robust circuit design against RTN.

Introduction

As device dimensions continuously shrink, the random telegraph noise (RTN) plays as one of the major challenges in robust circuit design. Most previous work focused on single-trap induced RTN, which reveals the physical switching behavior of oxide defects [1-9]. Nevertheless, even in highly-scaled devices, there are still possibilities to have more than one trap in a device due to the wide distribution of trap number per device [4], and more traps will be activated due to circuit aging [10-11]. However, very few studies on the multi-trap induced RTN have been reported [12-13]. And how the defects are coupled together should be further examined. Moreover, in practical digital operations, the trap behavior needs to be characterized under AC bias, as has been studied by AC STR and AC RTN methods by our group [6-9], and AC TDDS method by Grasser *et al.* [1-2]. But the frequency dependence of the defect coupling in multi-trap induced complex RTN under AC condition has not been reported yet.

In this paper, the coupling effects of multi-traps in complex RTN are experimentally studied in scaled high-κ/metal-gate MOSFETs for the first time. Challenges in characterizing coupled defects within different "test window" are addressed by extending DC/AC STR method. The bias and frequency dependences of defect coupling are extracted and discussed. And its impacts on circuit stability are also evaluated.

Devices and Characterization Method

The devices used in this work are planar high-κ/metal-gate nFETs with ultra-thin SiO_2/HfO_2. Compared with single-trap induced simple RTN, characterizing complex RTN is challenging, since each trap has its own "detectable window" in conventional DC RTN measurement [1-3]. For one given trap, as shown in Fig. 1, RTN signal cannot be observed outside its "detectable window", due to the huge deviation of capture and emission time at low/high V_G. Unfortunately, the detectable windows of each trap do not have large overlap with varying V_G in most cases, which makes the test window (for all traps) even narrower for characterizing complex RTN if using conventional DC RTN method measurement.

To overcome this problem, the statistical trap response (STR) method [6,8] is adopted here to expand the narrow test window to full V_G swing (*GND-VDD*). Fig.2 shows the schematics of DC/AC STR method. From recorded traces (Fig.3), the trap occupancy probability can be extracted, as shown in Fig.4 (DC) and Fig.5 (AC). By Eqs.1&2, the capture time constant can be obtained, as shown in Fig.6.

The DC STR method can be verified by comparing with DC RTN results within its test window. Fig.7 shows the capture time constants extracted by STR and conventional DC RTN. The two methods have the same trend and close values. The AC STR can be verified by comparing with advanced AC RTN method proposed by us recently [7,9]. Fig. 8 shows the typical results of AC RTN, and Fig. 9 shows good agreement between both methods within their overlap region. Therefore, the narrow DC RTN test window can be accurately expanded to full V_G swing by the proposed DC/AC STR method, as shown in Fig.10.

New Observations and Mechanism Analysis of Complex RTN

For complex RTN, we start from two-trap case. As shown in Fig.11, using conventional measurement, the complex RTN (with 4 levels induced by trap A and trap B) can be extracted only within the overlap of two individual trap windows. The coupling effect (the impact of trap B on trap A) can be obtained from extracting the trap A characteristics w/ or w/o trap B charged. The results show evident coupling on both RTN amplitude [Fig. 12(a)] and RTN time constants [Fig. 12(b)]. However, as expected, this complex RTN can be detected only in a narrow window (~50mV) using

conventional measurement, which is not suitable for studies within full V_G swing.

Therefore, STR method is extended from single-trap case to multi-trap here, as shown in Fig.13. The occupancy probability of both trap A and B can be directly extracted, which provides much larger V_G range than the conventional method (Fig.14). A valley in the occupancy probability can be clearly observed for both DC and AC conditions due to defect coupling effects, which deviates from the expected monotonic increasing trend in the single-trap case. This strong coupling region is interestingly found to be very close to the peak-G_m, which indicates that the defect coupling is correlated with current transport mechanism and will be discussed later.

To further study the impact of defect coupling on RTN time constants, a new extraction method is proposed (Fig.15). As shown in Fig. 16, the normalized impacts of coupling are plotted with varying V_G. Under DC condition, the defect coupling generally decreases with increasing V_G. However, the nonmonotonic peak can be observed near peak-G_m, which is consistent with Fig.14. Under AC condition, the impact of defect coupling decreases with increasing AC frequency, yet the impact is still non-negligible especially at low V_G (near V_{TH}).

The coupling effects between the two traps are fundamentally caused by the perturbation of the trap energy level (E_t) and the local carrier density (within the capture cross section of the trap) induced by the other trapped charge. The shift of E_t is most likely due to the Coulomb repulsion mechanism [14]. Take our result as an example, the occupation of trap *B* raises E_t of trap *A* by Coulomb repulsion, thus decreases the occupancy probability of trap *A*. With the increase of V_G, the Coulomb repulsion effect is weakened due to enhanced screening effect [14]. For the change of local carrier density, the blockade of one critical channel percolation path by other trap can be the possible mechanism, which will be discussed in detail below.

Due to the impacts of random discrete dopants in the channel (and other effects such as metal-gate workfunction variations), the surface potential is fluctuated, which results in current percolation paths from source to drain [15]. Fig.17 is an example from atomistic TCAD simulations, which shows the evolution of channel percolation paths formation from low V_G to high V_G. At the V_G near peak-G_m, the paths' number is the largest, and then the paths begin to merge together and finally become a whole sheet of inversion channel. That is why that the coupling between trap A and B has a peak near peak-G_m in Fig.16. The measured ΔI_d amplitude in Fig. 18, which shows a nonmonotonic trend with V_G, also confirms the formation of percolation paths in the channel [16]. As shown in Fig.19(a), at low V_G, trap B has little impact on the percolation path passing through trap A, thus the local current density under trap A does not change. With V_G increasing, more percolation paths are formed especially near peak-G_m , thus more than one paths could pass through trap A [Fig.19(b)]. Therefore, trap B can block the newly-formed path and reduces the local current density under trap A, which results in capture time increase of trap A. But under high V_G [Fig.19(c)], trap B can only reduce small amount of current due to the merging of percolation paths, and its impact on trap A is suppressed. Finally due to the enhanced screening effects combined with reduced percolation transport, the defect coupling is not obvious under very high V_G. That is why the peak in the defect coupling due to the perturbation of local current density is located around peak-G_m. Therefore, in general, the defect coupling is modulated by the two competitive mechanisms of Coulomb repulsion and the channel percolation (indicated by G_m), as shown in Fig.20.

Regarding the frequency dependence of defect coupling, Fig. 14 shows the reduced coupling between trap A and B with increasing *f*. Fig. 21 shows an extreme case, in which the slow trap H becomes inactive at higher *f*. When trap H is visible at DC or low *f*, it has impacts on the τ_c and the amplitude of the fast trap G; while when at higher *f*, there is no impacts of trap H on trap G. This can be understood in Fig. 22, where the effective occupation rate of slow trap H reduces fast (quickly below 1%) with increasing *f*, thus it is deactivated at high frequency.

Impacts of Complex RTN with Defect-Coupling on Circuit Stability

Based on the above new observations on complex RTN, its impacts on the stability of ring oscillators (RO) and SRAM cells are evaluated with defect coupling included. Fig.23 shows the period distributions of ROs, indicating reduced jitter if considering defect coupling. The read failure probability of SRAMs in Fig.24 also shows the reduced impacts of complex RTN if considering defect coupling. Therefore, there will be an underestimation of digital circuit transient performance if without including the defect coupling effect in complex RTN.

Summary

The defect coupling in complex RTN in high-κ/metal-gate devices are experimentally studied under full bias swing with extended STR method. The nonmonotonic bias-dependence of defect coupling is observed for the first time, which is found due to two competitive mechanisms. The trap interaction is observed to reduce with increasing frequency. The impacts of complex RTN on RO and SRAM stability are also evaluated, which show performance underestimation if not considering defect coupling. The results are helpful for future robust circuit design against RTN.

Acknowledgement: This work was partly supported by the 973 Projects (2011CBA00601), NSFC (61106085 and 60625403), and the National S&T Major Project (2009ZX02035-001). The authors would like to thank Prof. Tibor Grasser, Prof. Jiang Chen and Dr. H. Miki for the helpful discussions.

References: [1] T. Grasser, et al., ***Microelec.Reliab.***, p.39, 2011; [2] T. Grasser, et al., ***IEDM***, p.470, 2012; [3] H. Miki, et al., ***IEDM***, p.450, 2012; [4] K. Takeuchi, et al., ***VLSI***, p.53, 2009; [5] R. Huang, et al., ***Microelec. Reliab.***, p.1515, 2011; [6] C. Liu, et al., ***IEDM***, p.571, 2011; [7] J. Zou, et al., ***VLSI***, p.139, 2012; [8] C. Liu, et al., ***IEDM***, p.466, 2012; [9] J. Zou, et al., ***VLSI***, p.186, 2013; [10] B. Kaczer, et al., ***IRPS***, p.26, 2010; [11] C. Zhao, et al., ***IEEE T-ED***, p.1274, 2004; [12] E. Hsieh, et al., ***IEDM***, p.454, 2012; [13] N. Tega, et al., ***IEDM***, p.218, 2006; [14] M. Schulz, et al., ***APL***, p.2649, 1993; [15] A. Asenov, et al., ***IEEE T-ED***, p.839, 2003; [16] J. Franco, et al., ***IRPS***, 5A.4.1, 2012.

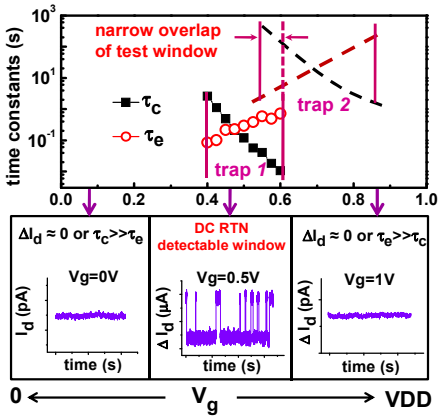

Fig. 1. Characterization of DC RTN using conventional method within full bias swing. RTN can be observed only in the "detectable window" due to the huge deviation of capture and emission time or small RTN amplitude at low/high V_g. For the case of complex RTN, detectable windows of each trap do not have large overlap in most cases, resulting in a narrow test window.

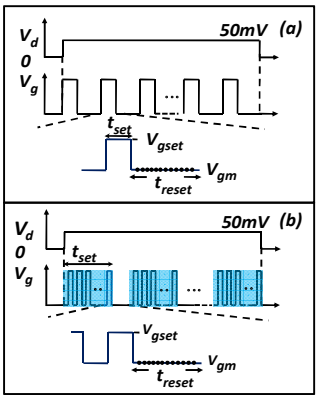

Fig.2. Measurement schematics of DC STR method (a) and AC STR method (b). The oxide trap is trapping during t_{set} and de-trapping during t_{reset}. The trap occupancy probability can be directly extracted from the recorded measurement traces.

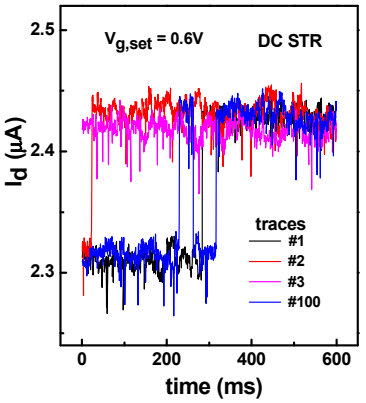

Fig. 3. Typical results of measurement traces under $V_{g,set}$ =0.6V (100 cycles) using the DC STR method. The step-like traces are caused by the random emission process of individual oxide trap.

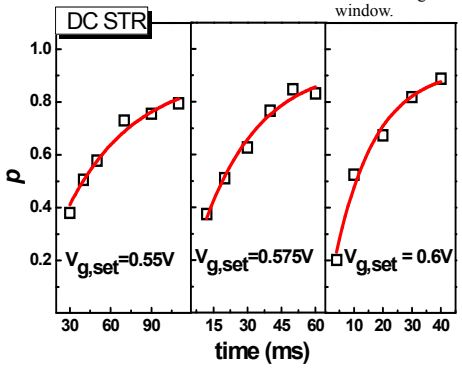

Fig.4. The trap occupancy probability p extracted from DC STR method under V_{gset}=0.55V, 0.575V, 0.6V, respectively. The symbols are the experiment data while the lines are fitting results using Eq.1.

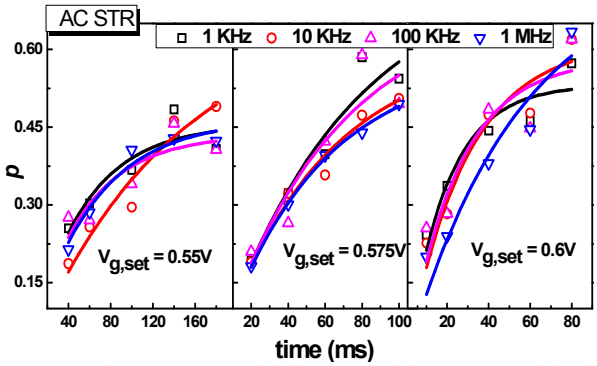

Fig. 5. The trap occupancy probability p extracted from AC STR method under V_{gset}=0.55V, 0.575V, 0.6V, respectively. AC frequency is from 1 KHz to 1 MHz. The symbols are the experiment data while the lines are fitting results using Eq.2.

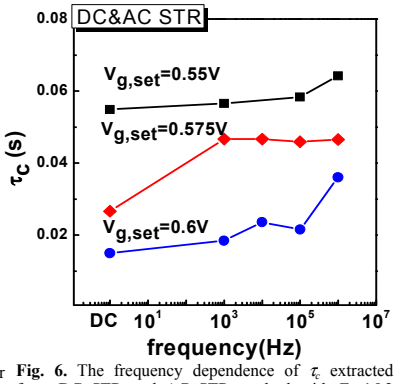

Fig. 6. The frequency dependence of τ_c extracted from DC STR and AC STR method with Eq.1&2 under the gate biases of 0.55V,0.575V, 0.6V, respectively.

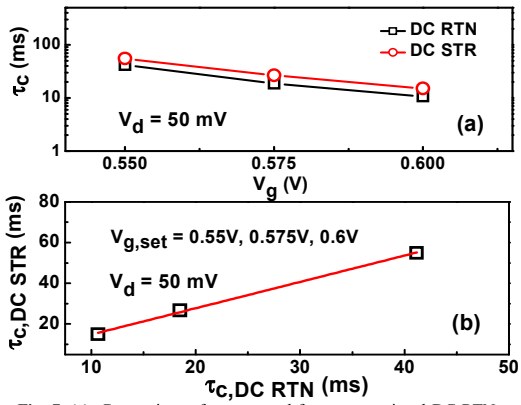

Fig. 7. (a): Comparison of τ_c extracted from conventional DC RTN and DC STR method. (b): τ_c extracted from DC STR shows linear relationship with DC RTN. Considering their relationship, the small deviations of the two methods can be corrected by a shift of system error.

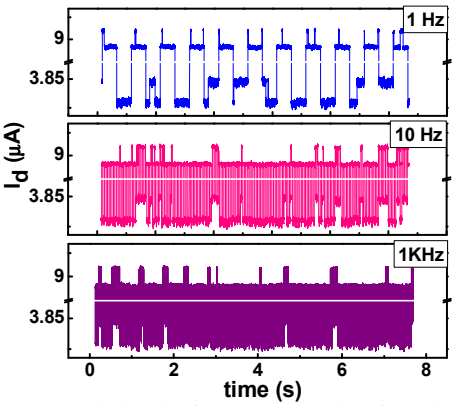

Fig. 8. Typical results of AC RTN under various frequencies. The high level of the AC signal is 0.575V, while the low level is 0.45V. Under both levels, RTN can be observed. V_d is 0.05V for all the cases.

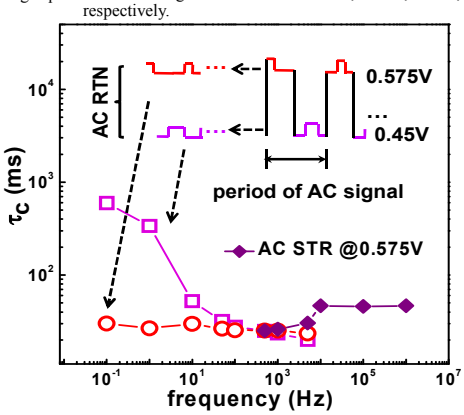

Fig. 9. Comparison of τ_c extracted by AC RTN (obtained from RTN at 0.45V and 0.575V respectively) and AC STR method. Good agreement between the two methods within the overlap region can be observed.

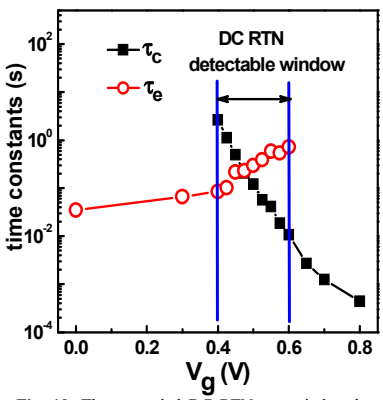

Fig. 10. The expanded DC RTN test window by the proposed STR method. DC RTN data is shown between the two bule lines.

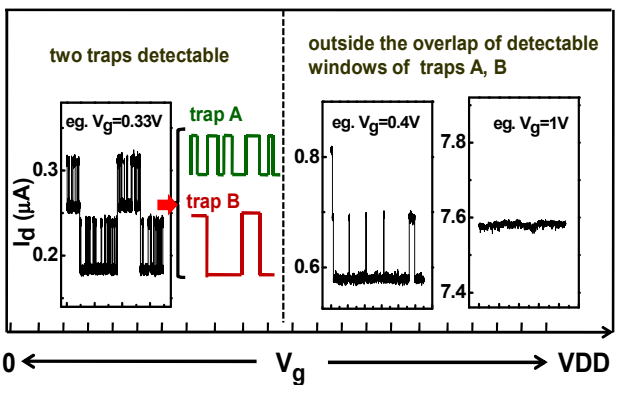

Fig.11. Characterization of the 4-level RTN (induce by trap A and B) using the conventional method. The complex RTN can be observed only within the overlap between two individual trap windows.

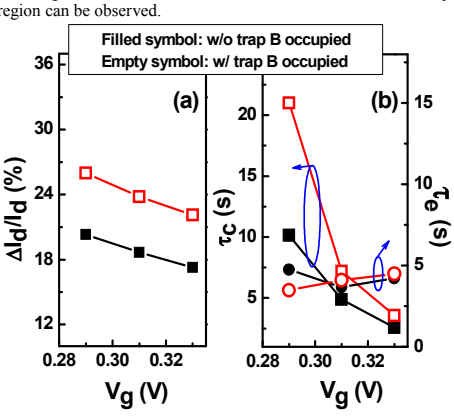

Fig. 12. Extracted RTN amplitude (a) and time constants (b) of trap A w. & w/o. trap B charged. Evident coupling effects can be found in both RTN amplitude and time constants.

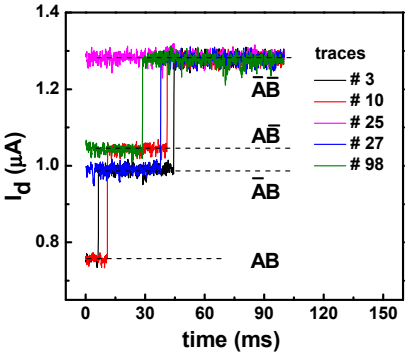

Fig. 13. Typical results of the measurement traces using STR method in case of complex RTN. Four levels can be seen ($\overline{A}\overline{B}$: both traps are not charged, $A\overline{B}$: only trap A is charged, $\overline{A}B$: only trap B is charged, AB: both traps are charged).

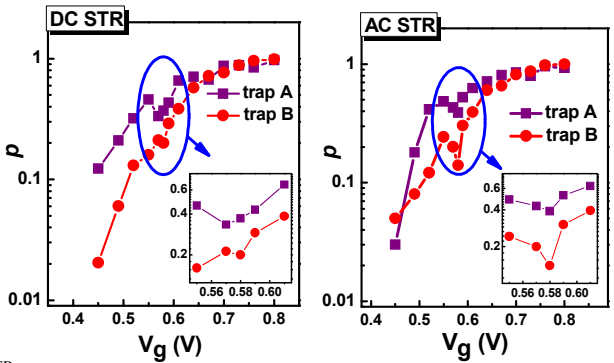

Fig. 14. The extracted occupancy probability of trap A and trap B based on DC & AC STR methods. A valley can be found around the G_m peak point for both DC and AC conditions due to the defect coupling effects.

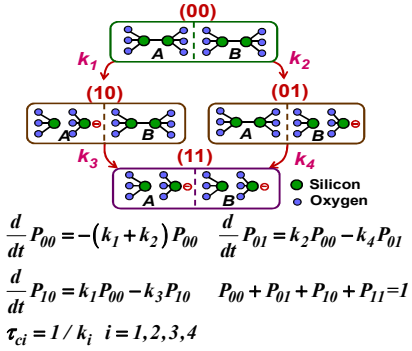

Fig. 15. Proposed extraction approach of time constant based on STR method. The four states are correlated to the observed current levels in Fig.13.

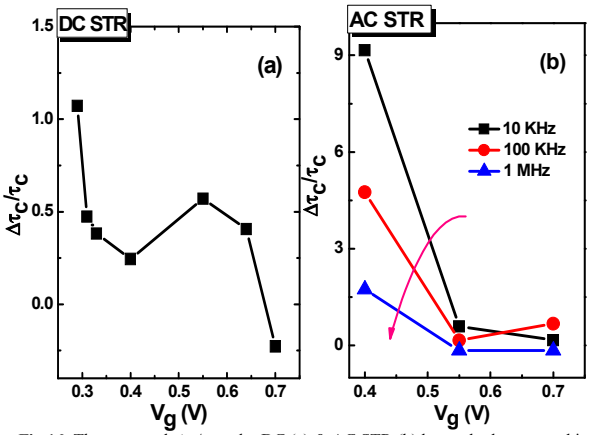

Fig.16. The extracted $\Delta\tau_c/\tau_c$ under DC (a) & AC STR (b) by methods proposed in Fig.15. $\Delta\tau_c = \tau_{c4} - \tau_{c1}$, which represents deviation of capture time (trap A) w/ or w/o the coupling effects of the other trap (trap B).

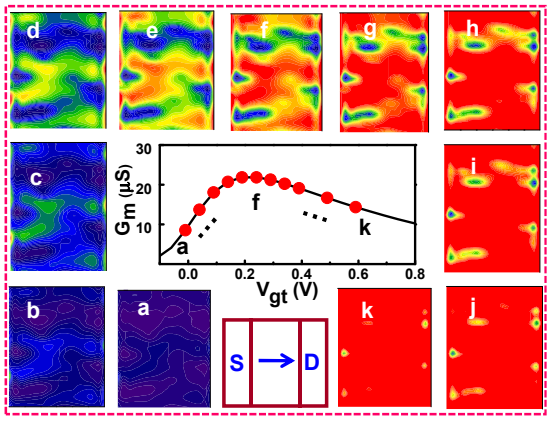

Fig. 17. Evolution of channel percolation paths formation from low V_g to high V_g. At the V_g near Gm peak point, the number of paths is largest, which indicates G_m value is positively correlated with the percolation paths.

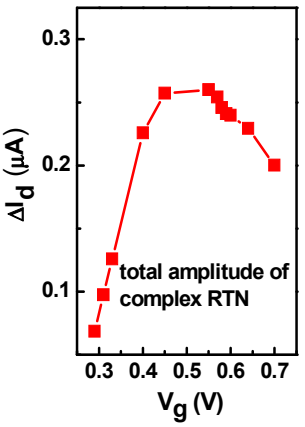

Fig.18. Total ΔI_d induced by trap A and B, which shows an abnormal nonmonotonic trend.

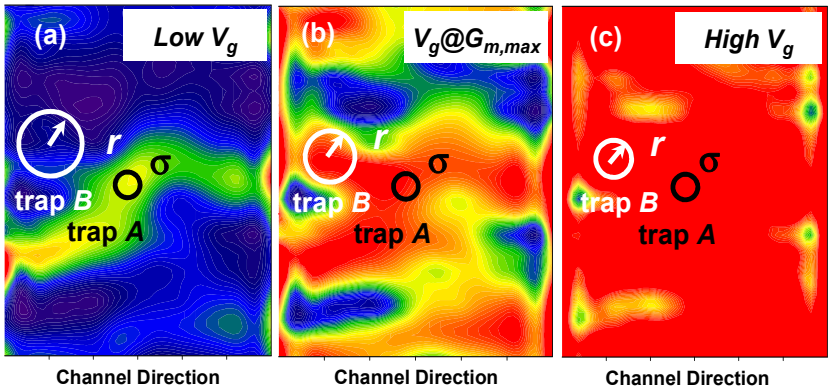

Fig. 19. Atomistic simulation results of the current density considering the random dopant induced percolation mechanism (a) at low V_g, (b) at V_g near G_m peak point (c) at high V_g. The percolation mechanism can dominate when V_g near G_m peak point. One newly-formed percolation path passing through trap A could be blocked by trap B, which will reduce the local carrier density of trap A, thus increase the capture time.

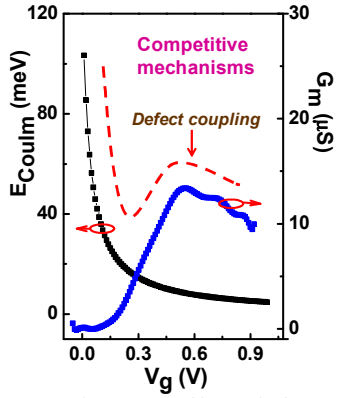

Fig.20. The two competitive mechanisms, Coulomb repulsion effects (Eq.3) and local carrier density perturbation (could have the same trend of $G_m \sim V_g$) .

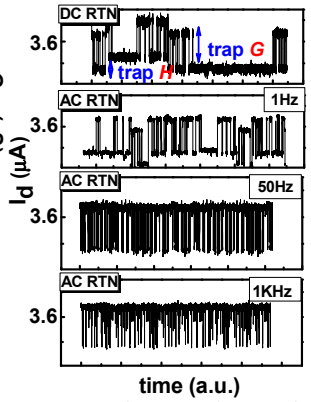

Fig. 21. Complex RTN under DC and AC condition in Device#6, which includes two traps (trap G and trap H). The high level of AC signal is 0.6V.

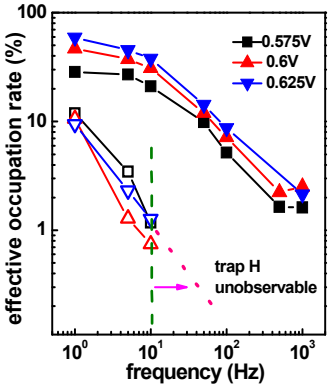

Fig.22. Frequency dependence of the extracted effective occupation rate of trap G and trap H. Trap H cannot be observed under higher frequency.

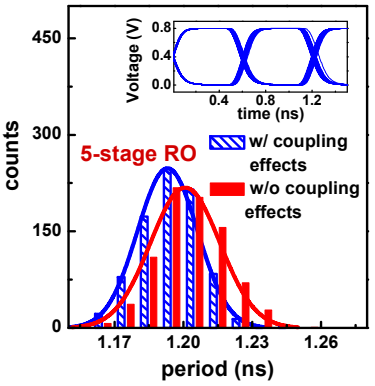

Fig. 23. Distributions of the periods in ring oscillator considering the impacts of complex RTN. Smaller variations can be found when considering coupling effects.

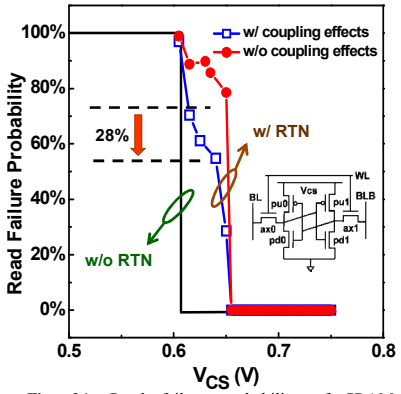

Fig. 24. Read failure probability of SRAM considering the impacts of complex RTN. About 28% overestimation can be found if not considering the coupling effects.

Eq.1 For DC STR extraction

$$p = \frac{\tau_e}{\tau_c+\tau_e}\left[1-exp\left(-\frac{\tau_c+\tau_e}{\tau_c\tau_e}t_{set}\right)\right]$$

Eq.2 For AC STR extraction

$$p = \frac{\tau_{eL}}{\tau_{cH}+\tau_{eL}}\left[1-exp\left(-\frac{\tau_{cH}+\tau_{eL}}{2\tau_{cH}\tau_{eL}}t_{set}\right)\right]$$

Eq.3 Coulomb repulsion of two traps

$$\tau_c = \tau_0\left\{1+exp\left[\left(E_t-E_f\right)/k_BT\right]\right\}$$

$$\tau_c' = \tau_0\left\{1+exp\left[\left(E_t-E_f+E_{Coulm}\right)/k_BT\right]\right\}$$

$$E_{Coulm} = \frac{q^2}{4\pi\varepsilon r_0}\left[1+\frac{qt_{inv}C_g}{4kT\varepsilon WL}\left(V_g-V_{FB}\right)\right]^{-1}$$